Inorganic Chemistry

Article

pubs.acs.org/IC

Synthesis, Structure, and Rigid Unit Mode-like Anisotropic Thermal Expansion of $BaIr_2In_9$

Nicholas P. Calta,[†] Fei Han,[‡] and Mercouri G. Kanatzidis*[,†,‡]

[†]Department of Chemistry, Northwestern University, Evanston, Illinois 60208, United States

[‡]Materials Science Division, Argonne National Laboratory, Argonne, Illinois 60439, United States

Supporting Information

ABSTRACT: This Article reports the synthesis of large single crystals of $BaIr_2In_9$ using In flux and their characterization by variable-temperature single-crystal and synchrotron powder X-ray diffraction, resistivity, and magnetization measurements. The title compound adopts the $BaFe_2Al_9$-type structure in the space group *P6/mmm* with room temperature unit cell parameters a = 8.8548(6) Å and c = 4.2696(4) Å. $BaIr_2In_9$ exhibits anisotropic thermal expansion behavior with linear expansion along the c axis more than 3 times larger than expansion in the *ab* plane between 90 and 400 K. This anisotropic expansion originates from a rigid unit mode-like mechanism similar to the mechanism of zero and negative thermal expansion observed in many anomalous thermal expansion materials such as ZrW_2O_8 and ScF_3.

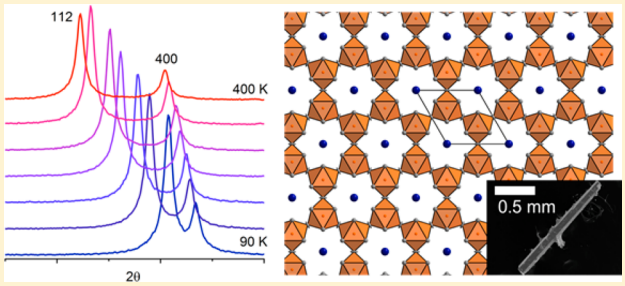

INTRODUCTION

Typical materials exhibit a positive coefficient of thermal expansion (CTE), namely, they expand when heated and contract when cooled. However, a small number of materials exhibit anomalous CTE values less than or equal to zero. Such materials are of significant research interest both from fundamental and applied perspectives.[1] Materials that exhibit zero or negative thermal expansion are particularly useful as components in composite structural materials when applications demand precisely controlled thermal expansion properties. New materials exhibiting unusual thermal expansion characteristics can provide insight into mechanisms of zero and negative thermal expansion (ZTE and NTE).

The microscopic mechanisms for anomalous thermal expansion materials vary significantly depending on the material in question. These mechanisms include magnetostriction in Invar alloys and Mn_3TN (T = Cu, Zn, Ga),[2] valence transitions,[3−5] structural effects near phase transitions,[6,7] and structural mechanisms based on particular features of the structure.[8−14] The most well-known example of a purely structure-based mechanism is the rigid unit mode (RUM) or "floppy mode" mechanism.[15−17] In this model, linear bridging atoms connect rigid structural units, and a low-frequency transverse phonon mode causes an overall reduction of the volume of the structure as the phonon amplitude increases with increasing temperature, pulling the two rigid units closer together. The RUM model is often invoked to describe ZrW_2O_8 and ScF_3, although the degree of actual rigidity of the oxide and fluoride polyhedra that comprise the rigid units in these two structures remains a matter of debate.[18,19] Other materials such as $SrAu_3Ge$[12] exhibit unidirectional NTE as a result of an accordion-like compression of a structural feature, in which strict bond-length requirements cause expansion along one direction to lead to contraction along another direction.

We discovered $BaIr_2In_9$ while exploring the Ba−Ir−In system using In flux, a synthetic technique that often leads to the discovery of complex intermetallics.[20−27] Three other compounds in this system are known: $BaIrIn_2$,[28,29] $BaIrIn_4$, and $Ba_2Ir_4In_{13}$.[30] All consist of a two- or three-dimensional Ir−In framework with Ba atoms filling the void spaces, and none exhibit direct Ir−Ir bonding. The title compound adopts the $BaFe_2Al_9$ structure type, a relatively rare structure reported for only eight compounds to date.[31−34] The most interesting feature of the structure is a linearly bridged, two-coordinate Ir−In−Ir bond. Different atoms in similar linearly bridged arrangements often lead to RUM-like effects that alter thermal expansion properties.[8,13] In spite of the unusual two-coordinate, linear bridging In atoms, no temperature-dependent structural investigations have been carried out in these compounds. This Article reports the synthesis and crystal structure of $BaIr_2In_9$, a new $BaFe_2Al_9$-type polar intermetallic compound. Physical property measurements indicate that $BaIr_2In_9$ is a diamagnetic metal that exhibits linear, anisotropic thermal expansion between 90 and 400 K.

EXPERIMENTAL METHODS

Synthesis. Large (up to 2 mm long) needle-like crystals of $BaIr_2In_9$ were prepared using the In flux method. All starting materials were used as received from the supplier, and all manipulations of air-sensitive Ba metal were carried out in a glovebox. One millimole of Ba metal dendrites (0.137 g, 99.9%, Sigma-Aldrich), 0.5 mmol of Ir

Received: June 25, 2015
Published: August 13, 2015

DOI: 10.1021/acs.inorgchem.5b01421
Inorg. Chem. 2015, 54, 8794−8799

Table 1. Single-Crystal Refinement Details for $BaIr_2In_9$ at Room Temperature[a]

empirical formula, Z	$BaIr_2In_9$, 1
formula weight	1555.12
temperature, wavelength	293(2) K, 0.71073 Å
crystal system	hexagonal
space group	$P6/mmm$ (No. 191)
unit cell dimensions (Å)	a = 8.8548(6), c = 4.2696(4)
unit cell volume (Å^3)	289.92(4)
calculated density (g/cm^3)	8.907
absorption coefficient (mm^{-1})	43.640
crystal size (μm)	80 × 30 × 20
theta range (deg)	4.60 to 34.86
index ranges	$-13 \le h \le 12$, $-14 \le k \le 13$, $-6 \le l \le 6$
reflections collected, independent	4322, 292 (R_{int} = 0.0553)
F(000)	651
completeness	99.7%
refinement method	full-matrix least-squares on F^2
data/restraints/parameters	292/0/14
goodness-of-fit	1.474
final R indices [$>2\sigma(I)$]	R_{obs} = 0.0236, wR_{obs} = 0.0569
R indices [all data]	R_{all} = 0.0236, wR_{all} = 0.0569
extinction coefficient	0.036(2)
largest diff. peak and hole (e·Å^{-3})	3.068 and −1.146

[a] $R = \sum||F_o| - |F_c||/\sum|F_o|$, $wR = (\sum[w(|F_o|^2 - |F_c|^2)^2]/\sum[w(|F_o|^4)])^{1/2}$, and calcd $w = 1/[\sigma^2(F_o^2) + (0.0163P)^2 + 3.7053P]$, where $P = (F_o^2 + 2F_c^2)/3$.

powder (0.096 g, 99.95%, American Elements), and 15 mmol of In lumps (1.722 g, 99.999%, Plasmaterials) were added to an alumina crucible with an inert cement base. The ratio used differs from the ideal ratio of 1 Ir/2 Ba in order to avoid the formation of $IrIn_3$. A corrosion-resistant stainless steel filter (McMaster-Carr, 100 mesh woven wire) was placed atop the crucible followed by a small length of alumina tube to serve as a counterweight. The entire apparatus was placed in a fused silica tube, evacuated to <10^{-3} mTorr, and sealed. The tube was heated to 1000 °C in 12 h, held at this temperature for 2 days, and then cooled to 650 °C in 2 days. After soaking at 650 °C for a few hours, the tube was quickly removed from the furnace and centrifuged to remove excess liquid In metal. This procedure produced brittle, rod-like hexagonal crystals both loosely adhered to the crucible walls and captured on the steel filter as well as a small amount of In not removed by centrifuging. Soaking products for a few hours in ∼10% HCl removed nearly all excess In metal. Some reaction mixtures contained a small amount (2−5%) of $IrIn_3$ as a second phase. $IrIn_3$ crystals have a significantly different morphology than that of $BaIr_2In_9$ crystals, so pure samples for physical properties measurements were easily obtained by individually selecting the desired crystals. Typical yields of $BaIr_2In_9$ were 50−70% based on the limiting reagent, Ba. The crystals are stable in humid air for at least 10 months.

Single-Crystal X-ray Diffraction. Single crystals with well-defined facets were selected and cut to an appropriate size for X-ray diffraction. They were screened for quality using a small number of diffracted frames on a Stoe IPDS2 single-crystal diffractometer equipped with graphite-monochromatized Mo Kα radiation (λ = 0.71073 Å). Full sphere data were collected on a few high-quality crystals. The data was reduced, integrated, and corrected for absorption using the Stoe X-Area suite.[35] The crystal structure was solved and refined with the SHELX package.[36] The initial collections were carried out at room temperature, and later data sets were collected at a variety of temperatures to investigate thermal expansion behavior.

Scanning Electron Microscopy−Energy Dispersive X-ray Spectroscopy (SEM-EDS). Scanning electron microscope (SEM) images and elemental compositions of synthesized crystals were obtained using a Hitachi S3400N-II scanning electron microscope equipped with an Oxford Instruments INCAx-act SDD EDS detector. Unpolished crystals mounted with carbon tape on an aluminum stub were imaged using an accelerating voltage of 20 kV. Spectra were collected at numerous clean crystal surfaces using 60 s acquisition times. The analyzed crystals yielded spectra with an average elemental composition of 75(1):9(1):16(2) (In/Ba/Ir), within error of the expected 75:8:17 ratio expected for a composition of $BaIr_2In_9$.

In-House Powder X-ray Diffraction. In order to determine reaction products, powder diffraction patterns of all reaction mixtures were collected. Portions of each reaction were ground to a powder and affixed to a borosilicate slide with double-sided tape. Diffraction patterns were measured in a reflectance geometry using an Inel CPS120 diffractometer equipped with Cu Kα radiation (λ = 1.5406 Å).

Synchrotron Powder X-ray Diffraction. In order to obtain a more precise CTE for $BaIr_2In_9$, high-resolution synchrotron powder X-ray diffraction patterns were collected at the Advanced Photon Source at Argonne National Laboratory using beamline 11-BM.[37] The sample consisted of ∼10 crystals individually picked, finely ground with a mortar and pestle, and sieved to particle sizes less than 90 μm in diameter. Since $BaIr_2In_9$ strongly absorbs X-rays, the sample was prepared using a coated capillary technique in which a kapton capillary was coated with nondiffracting grease (Dow Corning #4 electrical insulating compound) and then covered with the ground $BaIr_2In_9$ powder. After removing loose powder, the coated capillary was then contained in a second, larger kapton capillary and mounted in a base for measurement. The samples were spun at 60 Hz during measurement. Measurements used an average wavelength of 0.459004 Å. GSAS[38] and EXPGUI[39] were used to index and fit the data by Rietveld refinement using the single-crystal structure as a starting model.

Magnetization Measurements. Magnetization measurements as a function of temperature were measured using a Quantum Design PPMS-XL on a 7.0 mg sample of single crystals individually selected to avoid In contamination and then ground by mortar and pestle. The ground sample was glued into a gel capsule and contained in a straw.

Resistivity Measurements. Resistivity as a function of temperature was measured parallel to the c axis on oriented single crystals using a linear four-probe geometry on a Quantum Design PPMS. Contacts were made with gold wires attached to the sample using Dupont 4929N silver paste, and sample dimensions were measured using SEM images.

DOI: 10.1021/acs.inorgchem.5b01421
Inorg. Chem. 2015, 54, 8794−8799

RESULTS AND DISCUSSION

Structure. $BaIr_2In_9$ crystallizes in space group *P6/mmm* with the $BaFe_2Al_9$ structure type. The unit cell parameters determined from single-crystal diffraction at room temperature are a = 8.8548(6) Å and c = 4.2696(4) Å. Details of the single-crystal structural refinement are given in Table 1, and the refined structural model is shown in Figure 1. Four crystallographically independent atoms describe the structure (Table 2). $BaIr_2In_9$ is an intermetallic compound in which the electropositive Ba atoms occupy channels along the c axis and behave essentially as cations, donating their valence electrons to yield $Ba^{2+}[Ir_2In_9]^{2-}$. The remainder of the structure is a three-dimensional network of Ir and In atoms similar to bonding observed in other Ba−Ir−In phases.[28−30] This network has been previously described for $BaFe_2Al_9$ as a series of Al_6 octahedra that condense into an extended network.[40] An alternative view, which is more useful in the context of anisotropic thermal expansion, centers on $[IrIn_9]$ capped triangular prisms (Figure 1). Ir−In bond lengths range from 2.5564(2) Å for the capping bonds to 2.8825(6) Å for the other bonds. These triangular prisms stack in a face-sharing fashion along the c axis and connect in the ab plane by the equatorial capping In atoms. The capping In ligands form linear bridges with Ir−In−Ir angles of 180°. In addition to the relatively unusual linear two-coordinate environment of the capping In atom, its anisotropic displacement parameter is flat, disk-like, and perpendicular to the Ir−In−Ir bond (Table 3). This suggests the presence of a transverse phonon mode or modes that causes In to vibrate in the plane normal to the linear bridging bond. Such a transverse vibration is reminiscent of those present in materials that exhibit ZTE and NTE behavior as a result of rigid unit modes. Variable-temperature single-crystal X-ray diffraction data indicates that, while the c axis behaves normally in response to temperature, the a axis is nearly temperature-independent in the 100−300 K range within the resolution of our instrument. In order to further investigate the thermal expansion properties of $BaIr_2In_9$, we collected high-resolution synchrotron X-ray diffraction data to determine the unit cell parameters with greater certainty.

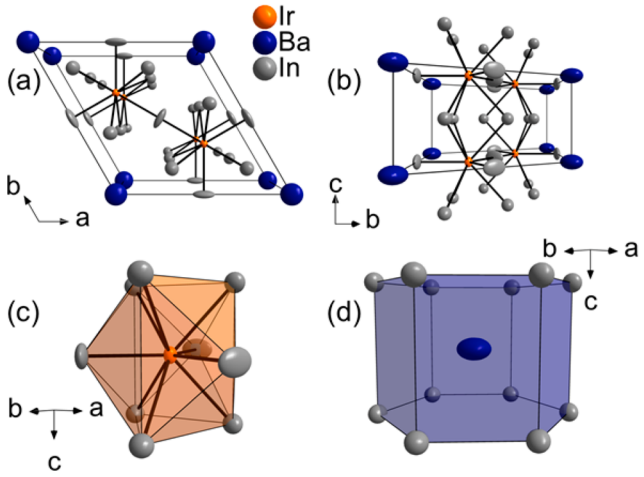

Figure 1. Structure of $BaIr_2In_9$ shown down the (a) c and (b) a axes. Also shown are the local coordination environments around the Ir (c) and Ba (d) atoms.

Table 2. Atomic Positions from the Single-Crystal Structural Refinement of $BaIr_2In_9$

atom	Wyckoff	x	y	z	U_{iso} (Å^2 × 10^{-3})
Ba	1a	0	0	0	23(1)
Ir	2c	2/3	1/3	0	4(1)
In1	6m	0.41409(9)	0.20705(4)	1/2	9(1)
In2	3f	0	1/2	0	14(1)

Table 3. Anisotropic Displacement Parameters (Å^2 × 10^{-3}) for $BaIr_2In_9$ at Room Temperature from Single-Crystal X-ray Diffraction[a]

atom	U_{11}	U_{22}	U_{33}	U_{12}	U_{13}	U_{23}
Ba	29(1)	29(1)	12(1)	14(1)	0	0
Ir	4(1)	4(1)	6(1)	2(1)	0	0
In1	9(1)	9(1)	9(1)	4(1)	0	0
In2	3(1)	22(1)	13(1)	2(1)	0	0

[a]The anisotropic displacement factor takes the form $-2\pi^2(h^2a^2U_{11} + k^2b^2U_{22} + \ldots + 2klbcU_{23})$.

Thermal Expansion. A typical synchrotron X-ray powder diffraction pattern is shown in Figure 2a,b, and additional fit details are given in the Supporting Information (Table S1) along with plots of each fitted temperature point (Figure S1). The patterns indicate that a small amount of In flux (~0.5%) is present in addition to $BaIr_2In_9$. Modeling the peak shape of $BaIr_2In_9$ proved to be rather difficult. A variety of common peak profiles provide only mediocre fits in both Le Bail and Rietveld refinements (Figure S2 in Supporting Information). The eventual best-fit solution was to include two $BaIr_2In_9$ phases with unit cell parameters, atomic positions, and displacement factors constrained to be equivalent, with peak profile terms allowed to vary. The primary difference between the two fitted sets of peak profile parameters was in terms describing Lorentzian broadening due to strain, suggesting two (or more) populations of differently strained $BaIr_2In_9$. We speculate that the presence of multiple strain populations arises from the synthetic procedure used to obtain $BaIr_2In_9$. The crystals obtained from the synthesis are almost always twinned or ingrown (Figure S3 in Supporting Information), so a rapid quench from 650 °C to room temperature during centrifugation coupled with the observed anisotropic thermal expansion could cause unusual strain in the resulting crystals. In spite of the difficulty of modeling strain properly in our sample, every attempt to model peak shape changed the refined unit cell parameters less than a single estimated standard deviation. Since d spacing dictates peak position and not peak shape, the unusual peak shapes observed do not affect our conclusions about thermal expansion. Synchrotron X-ray powder diffraction yields unit cell values that are significantly larger than the values obtained from single-crystal X-ray diffraction, but the CTE values when calculated by both methods are similar. We attribute this systematic difference to either extrinsic defects or a slight phase width that yields inhomogeneity from crystal to crystal.

We calculate CTE values using unit cells determined by powder diffraction using eq 1

$$\alpha_l = \frac{\Delta l/\Delta T}{l_0} \quad (1)$$

where α_l represents linear expansion coefficient, l represents a unit cell edge length, T represents temperature, and l_0

DOI: 10.1021/acs.inorgchem.5b01421
Inorg. Chem. 2015, 54, 8794−8799

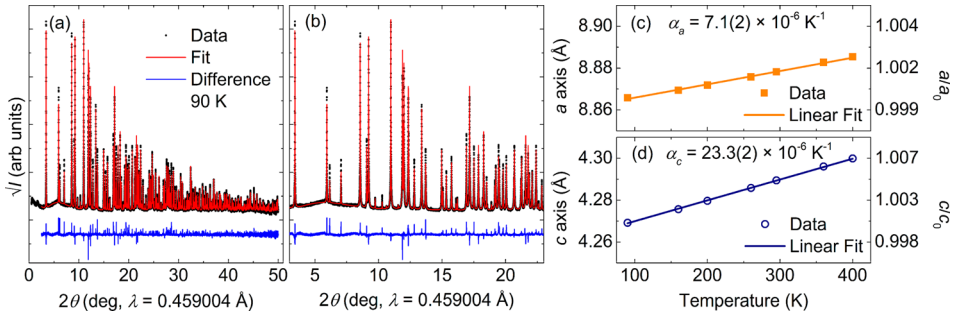

Figure 2. (a) Typical powder diffraction pattern collected at 90 K, with intensity shown on a square-root scale to emphasize small peaks. The small unfit features at low angle are a result of the Kapton sample holder. (b) Zoomed-in view of the same pattern shown in (a). (c, d) Unit cell parameters as a function of temperature extracted from synchrotron X-ray diffraction data by Rietveld refinement. Solid lines are linear fits to the data using eq 1 (see text).

represents the unit cell edge length at the base temperature of measurement. Figure 2c,d shows *a* and *c* axis lengths determined by synchrotron X-ray powder diffraction as a function of temperature. On the basis of these data, $\alpha_a = 7.1(2) \times 10^{-6}$ K^{-1} and $\alpha_c = 22.3(2) \times 10^{-6}$ K^{-1} in the temperature range 90−400 K. For comparison, $CeIrIn_5$ exhibits linear thermal expansion coefficients at 300 K of $\alpha_a \sim 12 \times 10^{-6}$ K^{-1} and $\alpha_c \sim 15 \times 10^{-6}$ K^{-1},[41] and $\alpha_l = 20.4(4) \times 10^{-6}$ K^{-1} for PbTe at 300 K.[42] Anisotropic expansion similar to what is observed in $BaIr_2In_9$ is unusual but not unprecedented in intermetallic compounds and is similar in magnitude to the thermal expansion behavior of Ti_5Si_3 ($\alpha_a \sim 5 \times 10^{-6}$ K^{-1} and $\alpha_c \sim 20 \times 10^{-6}$ K^{-1}),[43,44] although the mechanism for this anisotropy in Ti_5Si_3[45,46] differs from the mechanism that we propose for $BaIr_2In_9$.

The anisotropy in CTE and structural features give clues to the mechanism for thermal expansion in $BaIr_2In_9$ in the investigated temperature range. The strongest bonds present in $BaIr_2In_9$ form the Ir−In framework, so this framework must be responsible for the thermal expansion properties of the compound. The larger expansion along the *c* axis indicates that the [$IrIn_9$] polyhedra themselves expand significantly more than the *ab* plane suggests. However, the linearly bridged In atoms that link the columns of polyhedra in the *ab* plane exhibit a transverse, low-frequency phonon mode or modes (Figure 3).

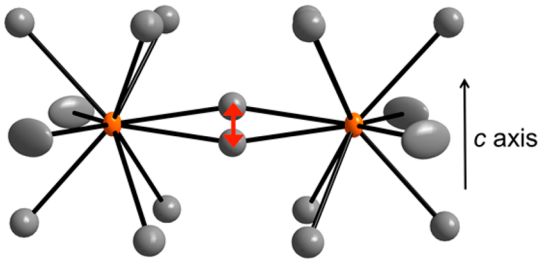

Figure 3. Schematic of the proposed In vibrational motion that causes the unusually small thermal expansion in the *ab* plane.

This vibrational motion increases in amplitude as the temperature increases, counteracting the normal expansion of the Ir−In framework in the *ab* plane. The flat, pancake-like anisotropic displacement parameter of this In atom observed in single-crystal X-ray diffraction further hints at the existence of this transverse vibration. While this behavior is very reminiscent of famous examples of RUM materials, it differs from classic RUM behavior because the [$IrIn_9$] units are not truly rigid. The displacement parameter of In1 is nearly isotropic, indicating that the vibrational motion that causes the pancake-like displacement parameter for In2 is not a result of correlated motion of the entire $IrIn_9$ polyhedron as a rigid unit. Instead, the vibration is mostly confined to motion of the Ir−In2−Ir bond. As this vibrational motion arises by virtue of the structure itself, it is most likely present in all $BaFe_2Al_9$-type compounds. Presumably, members of this family with a more rigid 3D network will exhibit greater degrees of anisotropic expansion. We plan to investigate this possibility in future experiments.

Physical Properties. Temperature-dependent magnetization measurements (Figure 4a) indicate that $BaIr_2In_9$ is diamagnetic, and the measurement shows a low-temperature upturn due to a small paramagnetic contaminant. Room temperature susceptibility is −0.00590(3) emu mol^{-1} Oe^{-1}. This means that for $BaIr_2In_9$ Landau diamagnetism is stronger than the Pauli paramagnetism often observed in polar intermetallic compounds. It also suggests a d^{10} configuration

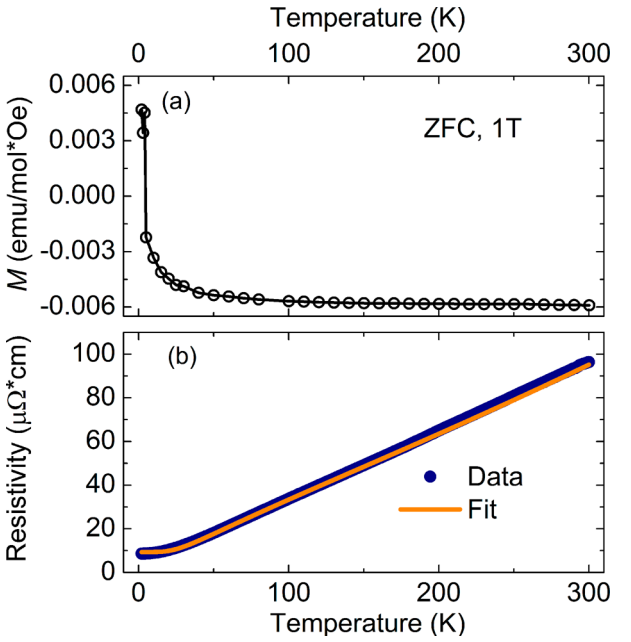

Figure 4. (a) Zero-field cooled magnetization data measured on a polycrystalline sample under an applied magnetic field of 1 T. The solid line is a guide to the eye. (b) Single-crystal resistivity measured along the *c* axis. Only crystal 1 is shown for clarity, and the fit shown is to the BGM model discussed in the text.

DOI: 10.1021/acs.inorgchem.5b01421
Inorg. Chem. 2015, 54, 8794−8799

Table 4. Residual Resistivity Ratio and BGM Fitting Parameters for $BaIr_2In_9$ Single Crystals

crystal	RRR (300 K/2 K)	ρ_0 ($\mu\Omega$ cm)	θ_D (K)	A ($\times 10^{-7}$ K^{-1})	K ($\times 10^{-13}$ K^{-3})
1	10.9	9.33(4)	154(1)	2.71(1)	2.08(3)
2	10.0	11.69(2)	181(1)	3.26(1)	1.41(2)

for Ir, implying a formal charge of at least Ir^{2-} as a result of electron transfer from Ba and the In framework. This observation is reasonable, as Ir is the most electronegative element present in the structure and therefore is likely to accept electrons from more electropositive neighbors.

Resistivity measurements between 2 and 300 K (Figure 4b) indicate that $BaIr_2In_9$ is a normal metal with no signs of strong electron correlation effects. Resistivity decreases with decreasing temperature until about 15 K, below which impurity scattering dominates and the resistivity plateaus. The data fit well to the Bloch–Grüneisen–Mott (BGM) model for electrical resistivity, given in eq 2[47]

$$\rho(T) = \rho_0 + AT\left(\frac{T}{\Theta_D}\right)^4 \int_0^{\Theta_D/T} \frac{x^4\,dx}{(e^x - 1)(1 - e^{-x})} + KT^3 \quad (2)$$

where T represents temperature, ρ_0 represents residual resistivity, θ_D represents the Debye temperature, x represents the possible phonon frequencies of the material, and A and K are scale factors. Crystal quality dictates ρ_0, with lower values indicating higher crystal quality, i.e., a lower concentration of point defects. This term determines the location of the low-temperature plateau in the resistivity and varies from crystal to crystal. The fifth-order term describes Umklapp electron–phonon scattering, the dominant mechanism of electron scattering at temperatures above the impurity regime. The cubic term describes Mott interband scattering, in which electrons scatter between different bands near the Fermi level.[48]

Fitted parameters and residual resistivity ratio (RRR = ρ_{300K}/ρ_{2K}) for two separate crystals are shown in Table 4. Both crystals are of relatively high quality, with ρ_0 values around 10 $\mu\Omega$ cm and RRR values of 10. For both crystals, the Umklapp term dominates the resistivity behavior, with only a negligible contribution from the Mott term, indicating that electron–phonon scattering dictates resistivity over the measured temperature range. The θ_D values are 154(1) K and 181(1) K, respectively, both well within the expected range for a heavy atom intermetallic with a relatively soft lattice. Extrinsic defects and experimental factors cause the difference in calculated Debye temperatures.

CONCLUSIONS

The new polar intermetallic compound, $BaIr_2In_9$, forms in good yield in molten In as a reactive solvent. It is a diamagnetic metal, suggesting a fully filled Ir 5d band. $BaIr_2In_9$ crystallizes in the hexagonal $BaFe_2Al_9$ structure type and exhibits anisotropic thermal expansion, with a linear thermal expansion coefficient in the *ab* plane 3 times smaller than the expansion observed along the *c* axis. This anisotropy is due to a rigid unit mode-like mechanism between the [$IrIn_9$] building blocks of the structure. While the [$IrIn_9$] units are not as rigid as would be anticipated for classic RUM behavior, the thermal expansion behavior is still dominated by transverse vibrational motion similar to what is observed in classical RUM materials. We speculate that such anomalous thermal expansion in the *ab* plane is likely a universal feature of the $BaFe_2Al_9$ structure type, as the mechanism of expansion is intimately linked to the structure itself.

ASSOCIATED CONTENT

Supporting Information

The Supporting Information is available free of charge on the ACS Publications website at DOI: 10.1021/acs.inorgchem.5b01421.

Additional details about Rietvelt refinement results and SEM images (PDF).

Single-crystal X-ray diffraction data (CIF).

AUTHOR INFORMATION

Corresponding Author

*E-mail: m-kanatzidis@northwestern.edu.

Notes

The authors declare no competing financial interest.

ACKNOWLEDGMENTS

Saul Lapidus, Matt Suchomel, and Lynn Ribaud provided assistance with data collection, experimental design, and interpretation of the synchrotron X-ray diffraction data. Use of the Advanced Photon Source at Argonne National Laboratory was supported by the U.S. Department of Energy, Office of Science, Office of Basic Energy Sciences, under Contract No. DE-AC02-06-CH11357. The work at Argonne National Laboratory was supported by the U.S. Department of Energy, Office of Science, Materials Sciences and Engineering. This work made use of the EPIC facility (NUANCE Center-Northwestern University), which has received support from the MRSEC program (NSF DMR-1121262) at the Materials Research Center; the International Institute for Nanotechnology (IIN); and the State of Illinois, through the IIN.

REFERENCES

(1) Evans, J. S. O. *J. Chem. Soc., Dalton Trans.* **1999**, 3317–3326.
(2) Takenaka, K.; Takagi, H. *Appl. Phys. Lett.* **2005**, *87*, 261902.
(3) Yamada, I.; Shiro, K.; Etani, H.; Marukawa, S.; Hayashi, N.; Mizumaki, M.; Kusano, Y.; Ueda, S.; Abe, H.; Irifune, T. *Inorg. Chem.* **2014**, *53*, 10563–10569.
(4) Peter, S. C.; Chondroudi, M.; Malliakas, C. D.; Balasubramanian, M.; Kanatzidis, M. G. *J. Am. Chem. Soc.* **2011**, *133*, 13840–13843.
(5) Azuma, M.; Chen, W.-t.; Seki, H.; Czapski, M.; Olga, S.; Oka, K.; Mizumaki, M.; Watanuki, T.; Ishimatsu, N.; Kawamura, N.; Ishiwata, S.; Tucker, M. G.; Shimakawa, Y.; Attfield, J. P. *Nat. Commun.* **2011**, *2*, 347.
(6) Zhao, Y.-Y.; Hu, F.-X.; Bao, L.-F.; Wang, J.; Wu, H.; Huang, Q.-Z.; Wu, R.-R.; Liu, Y.; Shen, F.-R.; Kuang, H.; Zhang, M.; Zuo, W.-L.; Zheng, X.-Q.; Sun, J.-R.; Shen, B.-G. *J. Am. Chem. Soc.* **2015**, *137*, 1746–1749.
(7) Chen, J.; Xing, X.; Sun, C.; Hu, P.; Yu, R.; Wang, X.; Li, L. *J. Am. Chem. Soc.* **2008**, *130*, 1144–1145.
(8) Margadonna, S.; Prassides, K.; Fitch, A. N. *J. Am. Chem. Soc.* **2004**, *126*, 15390–15391.
(9) Chapman, K. W.; Chupas, P. J.; Kepert, C. J. *J. Am. Chem. Soc.* **2006**, *128*, 7009–7014.

DOI: 10.1021/acs.inorgchem.5b01421
Inorg. Chem. 2015, 54, 8794–8799

(10) Goodwin, A. L.; Calleja, M.; Conterio, M. J.; Dove, M. T.; Evans, J. S. O.; Keen, D. A.; Peters, L.; Tucker, M. G. *Science* **2008**, *319*, 794−797.
(11) Mary, T. A.; Evans, J. S. O.; Vogt, T.; Sleight, A. W. *Science* **1996**, *272*, 90−92.
(12) Lin, Q.; Corbett, J. D. *J. Am. Chem. Soc.* **2012**, *134*, 4877−4884.
(13) Greve, B. K.; Martin, K. L.; Lee, P. L.; Chupas, P. J.; Chapman, K. W.; Wilkinson, A. P. *J. Am. Chem. Soc.* **2010**, *132*, 15496−15498.
(14) Chatterji, T.; Henry, P. F.; Mittal, R.; Chaplot, S. L. *Phys. Rev. B: Condens. Matter Mater. Phys.* **2008**, *78*, 134105.
(15) Tao, J. Z.; Sleight, A. W. *J. Solid State Chem.* **2003**, *173*, 442−448.
(16) Tucker, M. G.; Goodwin, A. L.; Dove, M. T.; Keen, D. A.; Wells, S. A.; Evans, J. S. O. *Phys. Rev. Lett.* **2005**, *95*, 255501.
(17) Ernst, G.; Broholm, C.; Kowach, G. R.; Ramirez, A. P. *Nature* **1998**, *396*, 147−149.
(18) Li, C. W.; Tang, X.; Muñoz, J. A.; Keith, J. B.; Tracy, S. J.; Abernathy, D. L.; Fultz, B. *Phys. Rev. Lett.* **2011**, *107*, 195504.
(19) Sanson, A. *Chem. Mater.* **2014**, *26*, 3716−3720.
(20) Chondroudi, M.; Balasubramanian, M.; Welp, U.; Kwok, W. K.; Kanatzidis, M. G. *Chem. Mater.* **2007**, *19*, 4769−4775.
(21) Peter, S. C.; Sarkar, S.; Kanatzidis, M. G. *Inorg. Chem.* **2012**, *51*, 10793−10799.
(22) Sebastian, C. P.; Malliakas, C. D.; Chondroudi, M.; Schellenberg, I.; Rayaprol, S.; Hoffmann, R. D.; Pottgen, R.; Kanatzidis, M. G. *Inorg. Chem.* **2010**, *49*, 9574−9580.
(23) Salvador, J. R.; Kanatzidis, M. G. *Inorg. Chem.* **2006**, *45*, 7091−7099.
(24) Bie, H. Y.; Tkachuk, A. V.; Mar, A. *J. Solid State Chem.* **2009**, *182*, 122−128.
(25) Bobev, S.; Hullmann, J.; Harmening, T.; Pottgen, R. *Dalton Trans.* **2010**, *39*, 6049−6055.
(26) Mathieu, J.; Achey, R.; Park, J. H.; Purcell, K. M.; Tozer, S. W.; Latturner, S. E. *Chem. Mater.* **2008**, *20*, 5675−5681.
(27) Zaremba, V. I.; Kalychak, Y. M.; Dubenskiy, V. P.; Hoffmann, R. D.; Rodewald, U. C.; Pottgen, R. *J. Solid State Chem.* **2002**, *169*, 118−124.
(28) Riecken, J. F.; Pöttgen, R. *Z. Naturforsch.* **2005**, *60b*, 118−120.
(29) Hoffmann, R.-D.; Pöttgen, R. *Chem. - Eur. J.* **2001**, *7*, 382−387.
(30) Palasyuk, A. M.; Corbett, J. D. *Inorg. Chem.* **2008**, *47*, 9344−9350.
(31) Manyako, I. B.; Yanson, T. I.; Zarechnyuk, O. *S. Izv. Akad. Nauk. SSSR, Metally* **1988**, 185−188.
(32) Turban, K.; Schäfer, H. *J. Less-Common Met.* **1975**, *40*, 91−96.
(33) Thiede, V.; Jeitschko, W. Z. *Z. Kristallogr. - New Cryst. Struct.* **1999**, *214*, 149−150.
(34) Lei, X.-W.; Zhong, G.-H.; Li, L.-H.; Hu, C.-L.; Li, M.-J.; Mao, J.-G. *Inorg. Chem.* **2009**, *48*, 2526−2533.
(35) *X-AREA*, version 1.39; STOE & Cie GmbH: Darmstadt, 2006 .
(36) Sheldrick, G. *Acta Crystallogr., Sect. A: Found. Crystallogr.* **2008**, *64*, 112−122.
(37) Wang, J.; Toby, B. H.; Lee, P. L.; Ribaud, L.; Antao, S. M.; Kurtz, C.; Ramanathan, M.; Von Dreele, R. B.; Beno, M. A. *Rev. Sci. Instrum.* **2008**, *79*, 085105.
(38) Larson, A. C.; Von Dreele, R. B. *General Structure Analysis System (GSAS): Los Alamos National Laboratory Report LAUR 86-748*; Los Alamos National Laboratory: Los Alamos, NM, 2000.
(39) Toby, B. *J. Appl. Crystallogr.* **2001**, *34*, 210−213.
(40) Vajenine, G. V.; Hoffmann, R. *J. Am. Chem. Soc.* **1998**, *120*, 4200−4208.
(41) Takeuchi, T.; Inoue, T.; Sugiyama, K.; Aoki, D.; Tokiwa, Y.; Haga, Y.; Kindo, K.; Ōnuki, Y. *J. Phys. Soc. Jpn.* **2001**, *70*, 877−883.
(42) Houston, B.; Strakna, R. E.; Belson, H. S. *J. Appl. Phys.* **1968**, *39*, 3913−3916.
(43) Thom, A. J.; Akinc, M.; Cavin, O. B.; Hubbard, C. R. *J. Mater. Sci. Lett.* **1994**, *13*, 1657−1660.
(44) Zhang, L.; Wu, J. *Scr. Mater.* **1997**, *38*, 307−313.
(45) Schneibel, J. H.; Rawn, C. J. *Acta Mater.* **2004**, *52*, 3843−3848.
(46) Fu, C. L.; Wang, X.; Ye, Y. Y.; Ho, K. M. *Intermetallics* **1999**, *7*, 179−184.
(47) Mizutani, U. *Introduction to the Electron Theory of Metals*; Cambridge University Press: Cambridge, UK, 2001.
(48) Mott, N. F.; Jones, H. *The Theory of the Properties of Metals and Alloys*; Oxford University Press: New York, 1958.

DOI: 10.1021/acs.inorgchem.5b01421
Inorg. Chem. 2015, 54, 8794−8799